Supporting information for: Ab initio calculations of ultra-short carrier dynamics in 2D materials: valley depolarization in single-layer WSe_2

Alejandro Molina-Sánchez,*,†,‡ Davide Sangalli,¶ Ludger Wirtz,† and Andrea Marini¶

†*Physics and Materials Science Research Unit, University of Luxembourg, 162a avenue de la Faïencerie, L-1511 Luxembourg, Luxembourg*

‡*Materials Science Institute, University of Valencia, P.O. Box 22085, E-46071 Valencia, Spain*

¶*CNR-ISM, Division of Ultrafast Processes in Materials (FLASHit), Area della Ricerca di Roma 1, Monterotondo Scalo, Italy*

E-mail: alejandro.molina@uv.es

Methods

Equilibrium properties. Equilibrium properties are computed starting from a self–consistent calculation of the Kohn–Sham (KS) eigenvalues and eigenstates in the framework of Density–Functional Theory (DFT) within the local-density approximation (LDA). DFT and Density Functional Perturbation Theory (DFPT) calculations have been performed with the `PWSCF` code.[S1] The spin–orbit interaction is fully considered, using spinorial wave function and rel-

ativistic norm–conserving pseudopotentials. The plane wave energy cut-off used is 110 Ry and the charge density is calculated on a $12 \times 12 \times 1$ **k**-grid. The LDA band gap is corrected by 1.04 eV. This scissor shift has been calculated within the GW approximation for the electronic self–energy[S2] coded in the `YAMBO` code,[S3] using a Coulomb cutoff to prevent electron-electron interaction between neighboring layers.[S4] Fig. S1 shows the band structure of single layer WSe_2. The large spin–orbit correction of the valence band at K appears clearly. In contrast, the spin–orbit coupling has a smaller effect on the conduction band, even if it remains important for the correct description of the material.[S5] The electronic band structure shows a local maximum at Γ, 200 meV below of the conduction band maximum at K. The conduction band, instead, has secondary minimum between K and Γ, and M and Γ. As shown in the main text, the topology of the band structure favors valley depolarization in the conduction band and it makes the carrier dynamics slower in the valence bands, especially at low temperatures.

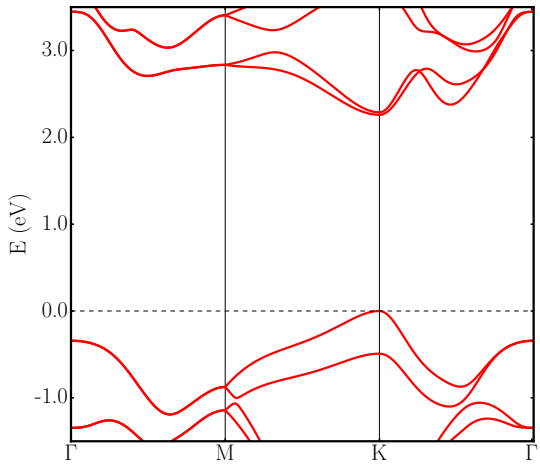

Figure S1: Quasi–particle band structure of a single layer of WSe_2. The energies are obtained by means of the *GW* approximation applied on top of the DFT–LDA energy levels.

The optical absorption (see Fig. 1(b) in main text) is obtained from the solution of the KBE, as implemented in the `YAMBO` code.[S3] This is used to determine the energy position of the A exciton. This frequency will be used as the pump pulse frequency in the non equilibrium simulation. The peak A is converged using two valence and two conduction bands in a $24 \times 24 \times 1$ **k**-grid. It is worth to mention that a convergence of the full spectra

would require more bands and a $60 \times 60 \times 1$ $\mathbf{k}$-grid.[S6,S7] Since the energy of the pump probe is tuned to the position of the A exciton peak, peak C is hardly involved in the carrier dynamics and we have opted for an intermediate solution which combines accuracy and feasible computational costs. We construct the equilibrium density matrix of the system in the KS space $\rho_l\left(t=0\right)$ which we use as a starting condition for the real–time propagation of Eq.(1) of the main text.

Non–equilibrium dynamics: the coherent term. The term in Eq. (1) of the main text that describes the interaction with the external laser pulses and the coherent correlation effects is

$$\partial_t \rho\left(\tau\right)_l\big|_{coh} = \epsilon_l \rho\left(\tau\right)_l + \left[\Delta\Sigma^{Hxc}, \rho\right]_l + \left[U\left(\tau\right), \rho\right]_l . \tag{1}$$

Here $\epsilon_l = (\epsilon_{n\mathbf{k}} - \epsilon_{m\mathbf{k}})$ are the energy differences between the quasi–particle eigenenergies of the equilibrium system (without any applied field). $\Delta\Sigma_l^{Hxc}$ is the variation of the Hartree potential plus the exchange and correlation self–energy at time τ. $U_l = -V\,\mathbf{E}\left(\tau\right)\cdot\mathbf{P}_l$ is the potential given by the circularly polarized pump pulse. V is the volume of the unit cell, $\mathbf{E}(\tau)$ is the electric field, and $\mathbf{P}_l$ is the vector of the dipole matrix elements. The $U_l\left(\tau\right)$ term drives the system excitation in a dipole approximation while the term $\left[\Delta\Sigma^{Hxc}, \rho\right]_l$ accounts for the electron–hole interaction during the photo–excitation process and the subsequent depolarization,[S8] by including excitonic effects to linear order. The dipole approximation is well justified in the energy range of few eV, since the experimental laser field used has a wave–length much larger than the unit cell. It implies that the photoexcited population is created at negligible transfered momentum, i.e., negligible momentum difference between the electron and the hole.

Non–equilibrium dynamics: the collision term. The dissipation term $\partial_t \rho\left(\tau\right)_l\big|_{coll}$ is the only term in the equation for ρ that depends explicitly on the sample temperature T, while $\partial_t \rho\left(\tau\right)_l\big|_{coh}$ has only an implicit dependence trough ρ. $\partial_t \rho\left(\tau\right)_l\big|_{coll}$ includes the scatter-

ing mechanisms relevant for the valley pseudospin polarization dynamics. It reads:[S9,S10]

$$\partial_t \rho\left(\tau\right)_l\big|_{coll} = \sum_J \left[-\gamma_l^{(e,J)}\left(\tau,T\right)\rho_l\left(\tau\right) + \gamma_l^{(h,J)}\left(\tau,T\right)\bar{\rho}_l\left(\tau\right)\right], \tag{2}$$

with $\bar{\rho}_l = \delta_{n,m} - \rho_l$. The sum runs over $J = e-p, e-e, e-\gamma$, the three possible scattering channels: electron–phonon, electron–electron and electron–photon. γ_l are the generalized non–equilibrium lifetimes whose definition will be given below.

The steps that lead to Eq. (2) can be found in Ref. S9. The derivation starts from the exact definition of the two–times collision term $\partial_t G_l^<\left(t,t'\right)\big|_{coll}$, with $G^<$ the exact two–times lesser Green's function[S11] and uses a controlled series of approximations: (i) the generalized Kadanoff–Baym ansatz[S11] is used to close the equation of motion and write it as a functional of the density matrix, (ii) memory effect are neglected during the scattering process, (iii) the off–diagonal matrix elements of ρ are assumed to be negligible (quasi–adiabatic approximation), (iv) the retarded and advanced Green functions, which are also needed to derive the collision term, are assumed to have a QP form constructed from the QP eigenvalues and lifetimes. Under these approximations the scattering term assumes a form which is equivalent to the scattering term of the semi–classical Boltzmann equation. We underline that the resulting lifetimes appearing in Eq. (2) are time dependent and updated during the dynamics.[S12] Eq. (2) goes well beyond the relaxation time approximation that, being band and **k**–point independent, does not allow any inter–valley scattering.

The explicit form of the electron–phonon non–equilibrium lifetimes. The final form of the lifetimes depends on the approximation used for the self–energy. In the present approach and in the `Yambo`[S3] code, the generalized[S10] *GW* approximation is used for all self–energies (electron–electron, electron–phonon and electron–photon). In the electron-phonon case, the *GW* approximation corresponds to the well known Fan self–energy.[S13] Within this approximation the lifetimes of Eq. (2) can be expressed in terms of

$\gamma_l^{(i),(e-p)} = (\gamma_{n\mathbf{k}}^{(i)} + \gamma_{m\mathbf{k}}^{(i)})/(1+\delta_{n,m})$. The scattering rates of electron and holes are given by

$$\gamma_{n\mathbf{k}}^{(e)} = \frac{\pi}{N}\sum_{\lambda\mathbf{q}m} |g_l^{\mathbf{q}\lambda}|^2 \left[P(\epsilon_{l\mathbf{q}} - \omega_{\lambda\mathbf{q}}, \gamma_{l\mathbf{q}}^0)\, f_{m\mathbf{k}+\mathbf{q}}^{(h)}(N_{\lambda\mathbf{q}}+1) + P(\epsilon_{l\mathbf{q}} + \omega_{\lambda\mathbf{q}}, \gamma_{l\mathbf{q}}^0)\, f_{m\mathbf{k}+\mathbf{q}}^{(h)} N_{\lambda\mathbf{q}}\right], \quad (3)$$

$$\gamma_{n\mathbf{k}}^{(h)} = \frac{\pi}{N}\sum_{\lambda\mathbf{q}m} |g_l^{\mathbf{q}\lambda}|^2 \left[P(\epsilon_{l\mathbf{q}} + \omega_{\lambda\mathbf{q}}, \gamma_{l\mathbf{q}}^0)\, f_{m\mathbf{k}+\mathbf{q}}^{(e)}(N_{\lambda\mathbf{q}}+1) + P(\epsilon_{l\mathbf{q}} - \omega_{\lambda\mathbf{q}}, \gamma_{l\mathbf{q}}^0)\, f_{m\mathbf{k}+\mathbf{q}}^{(e)} N_{\lambda\mathbf{q}}\right]. \quad (4)$$

Here $\epsilon_{l\mathbf{q}} = \epsilon_{m\mathbf{k}+\mathbf{q}} - \epsilon_{n\mathbf{k}}$ and $\gamma_{l\mathbf{q}}^0 = \sum_{i,J} \gamma_{m\mathbf{k}+\mathbf{q}}^{0,(i),(J)} + \gamma_{n\mathbf{k}}^{0,(i),(J)}$ are the equilibrium quasi–particle energies and lifetimes. The latter are described with a term proportional to the density of states for the electron-phonon channel. $g_l^{\mathbf{q}\lambda} = g_{nm\mathbf{k}}^{\mathbf{q}\lambda}$ are the first order electron–phonon matrix elements, which represent the general scattering amplitude of a process where an electron(hole) in the state n jumps to the state m with the emission or absorption of a phonon with energy $\omega_{\lambda\mathbf{q}}$. $N_\lambda(\mathbf{q})$ is the phonon population, described by a Bose–Einstein distribution function. The lifetimes defined by Eqs. (3) and (4) are the sum of emission and absorption processes. The emission term is weighted by the $(N_\lambda(\mathbf{q})+1)$ prefactor and describes also the spontaneous emission of phonons at zero temperature, where $N_\lambda(\mathbf{q}) = 0$. The functions P describes the energy conservation during emission/absorption and results from the fourier transform of the product of two quasi–particle Green functions. It has an hyperbolic–secant form which reduces to the standard QP dependence $e^{-\gamma_{n\mathbf{k}}^{(i)} t}$ for long times, but also correctly describes the gaussian $t \to 0$ limit. We refer to this approximation as hyperbolic–secant quasi–particle (HS–QP) approximation:

$$P(\omega, \Gamma) = \frac{4\pi\omega}{\gamma^2} \frac{1}{\cosh(\frac{\pi\omega}{2\Gamma})}. \quad (5)$$

Electron–phonon vs exciton–phonon non–equilibrium lifetimes. The electron and hole lifetimes in Eqs. (3)-(4) describe one electron (hole) scattering from the state $n\mathbf{k}$ to the state $m\mathbf{k}+\mathbf{q}$ due to the electron-phonon interaction. Such a picture would be exact in a system of non-interacting electrons (holes) or in case a single electron (hole) is added to the ground state. In such case the energy of the system before and after the scattering would be

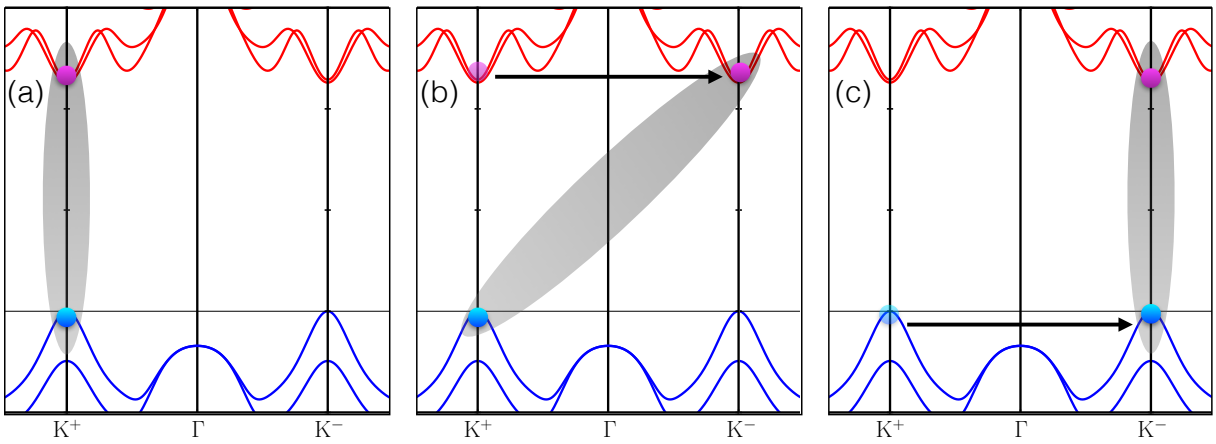

Figure S2: Representation of the two steps making an exciton scatter from $\{K, q = 0\}$ scatter to $\{K', q = 0\}$ via exciton-phonon coupling. First the electron in conduction band (frame a) moves from K to K', thus creating an exciton with momentum $q = K - K' = K$, i.e. $\{K, K - K'\}$, which has the same binding energy (frame b). Second also the hole scatters from K to K' (frame c). This two steps process underlines the composite nature of the exciton-phonon interaction as a sum of electron-phonon and hole-phonon interaction.

well described by $E_I^{N+1} \approx E_0^N + \epsilon_{n\mathbf{k}}$ and $E_J^{N+1} \approx E_0^N + \epsilon_{m\mathbf{k+q}}$. The energy difference between the two states would be $E_I^{N+1} - E_J^{N+1} \approx \epsilon_{n\mathbf{k}} - \epsilon_{m\mathbf{k+q}}$. However, the system we describe after the action of the pump pulse is in the excited state of $E_I^N \approx E_0^N + \omega_{\gamma 0}$, with $\omega_{\gamma 0}$ matching the laser pulse energy. The number of particles being conserved during the scattering process, all the subsequent states will have energy $E_J^N \approx E_0^N + \omega_{\gamma'\mathbf{q}}$. Thus the change in energy of the system is $E_I^N - E_J^N \approx \omega_{\gamma 0} - \epsilon_{\gamma'\mathbf{q}}$. In WSe_2 electrons and holes strongly interact, with a binding energy of about 0.5 eV. Accordingly one would expect $\omega_{\gamma 0} - \omega_{\gamma'\mathbf{q}}$ to be very different from $\epsilon_{n\mathbf{k}} - \epsilon_{m\mathbf{k+q}}$. However this is not the case.

In this manuscript, we only need the energy of the excitons A and B, for $\mathbf{q} \approx 0$ and $\mathbf{q} \approx K$ (see Fig. S2). The wave function of these excitons is very localized in transition space

$$|\gamma\mathbf{q}\rangle \approx |v\mathbf{k}\rangle \times |c\mathbf{k} + \mathbf{q}\rangle \tag{6}$$

so that in practice we can identify the exciton with a specific transition: let us use the

notation $|\gamma\mathbf{q}; cv\mathbf{k}\rangle$. Its energy can be written as

$$\omega_{\gamma\mathbf{q};cv\mathbf{k}} \approx (\epsilon_{c\mathbf{k}+\mathbf{q}} - \epsilon_{v\mathbf{k}}) + \langle v\mathbf{k}, c\mathbf{k}+\mathbf{q}|K^{eh}|v\mathbf{k}, c\mathbf{k}+\mathbf{q}\rangle \tag{7}$$

with K^{eh} the BSE kernel. Finally, it has been shown[S14] that

$$\langle v\mathbf{k}, c\mathbf{k}+\mathbf{q}|K|v\mathbf{k}, c\mathbf{k}+\mathbf{q}\rangle \approx \langle v\mathbf{k}, c\mathbf{k}+\mathbf{q}'|K^{eh}|v\mathbf{k}, c\mathbf{k}+\mathbf{q}'\rangle \tag{8}$$

for $(\mathbf{q}-\mathbf{q}') = K$, i.e. for the inter-valley scattering processes we consider in the present work. Using these results the two exciton-phonon scattering process represented in Fig. S2 can be desribed as follow. First the system jumps from the state $\omega_{\gamma 0;K}$ to the state $\omega_{\gamma K;K}$ with an electron jumping from K to K' and the hole remaining as a spectator. Later the system jumps from $\omega_{\gamma K;K}$ to $\omega_{\gamma 0;K'}$ with a hole jumping from K to K' and the electron remaining as a spectator. Indeed the energy conservation becomes

$$P\Big((\omega_{\gamma 0;K} - \omega_{\gamma K;K}) \pm \omega_{\lambda K}, \Gamma\Big) \approx P\Big((\epsilon_{cK'} - \epsilon_{cK}) \pm \omega_{\lambda K}, \Gamma\Big) \tag{9}$$

$$P\Big((\omega_{\gamma K;K} - \omega_{\gamma 0;K'}) \pm \omega_{\lambda K}, \Gamma\Big) \approx P\Big((\epsilon_{vK'} - \epsilon_{vK}) \pm \omega_{\lambda K}, \Gamma\Big) \tag{10}$$

and the matrix elements between the two excitonic states are well approximated as

$$\langle \gamma 0; K|\partial V^{SCF}|\gamma K; K\rangle \approx \langle vK|vK\rangle g^{\lambda K}_{ccK} \tag{11}$$

$$\langle \gamma K; K|\partial V^{SCF}_{\lambda K}|\gamma 0; K'\rangle \approx \langle cK'|cK'\rangle g^{\lambda K}_{vvK}. \tag{12}$$

These are exactly the terms entering the electron and hole lifetimes in Eqs. (3)-(4). We have performed a numerical comparison of the exciton-phonon and electron-phonon scattering rate from K to K'. We find that the electron-phonon and exciton-phonon lifetimes are similar. However a complete calculation of the exciton-phonon lifetimes requires to obtain the exciton dispersion in the full Brillouin zone and this is beyond the scope of the present

work.[S15]

Electron-phonon matrix elements.

The matrix elements $g_l^{\mathbf{q}\lambda}$ are calculated on the same grid as the Bethe–Salpeter equation ($24 \times 24 \times 1$), by using the Density–Functional Perturbation Theory as implemented in the Quantum Espresso[S1] code.

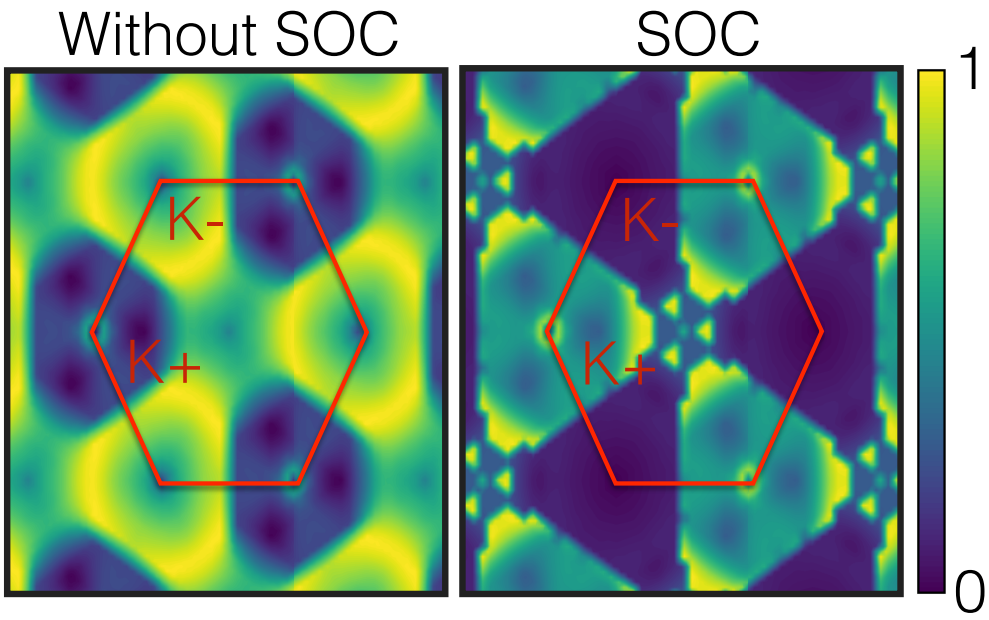

Figure S3: Electron-phonon matrix elements $|g^{\mathbf{q}}_{nn'\mathbf{k}}|^2$, as a function of the phonon momentum $\mathbf{q}$. We have chosen $\mathbf{k} = \mathbf{K}^+$ and $n = n'$ equal to the top valence band. The left/right frames show calculations without/with spin-orbit interaction.

In Fig. S3 we represent the matrix elements $|g_l^{\mathbf{q}\lambda}|^2$ for $n = n'$ with n the top valence band, $\mathbf{k} = \mathbf{K}^+$ and with $\mathbf{q}$ running all over the Brillouin zone. Physically this plot represents the scattering probability for the valence holes at K^+ to scatter and jump to other points. In Fig. S3 we consider a calculation without (left frame) and with (right frame) SOC included. We clearly see that in the case without SOC the inter–valley scattering $K^+ \to K^-$ is possible. The SOC is responsible for the dramatic decrease of the inter–valley scattering probability. This decrease is the driving force that motivates the slow regime of the dynamics observed experimentally. On the contrary, in the case of the conduction states, the SOC splitting is much smaller and allows for an efficient and direct inter–valley scattering.

Parameters of the carrier dynamics calculation. We would like to distinguish

between experimental and convergence parameters. The experimental parameters are set by the experimentalists and serve as input to our simulation. They are the pump damping (100 fs), the temperature, (ranging from 4 K up to 150 K), the laser intensity (10^5 kW/m^2), the pump frequency (1.68 eV). The set of simulations parameters must be obtained through a convergence study. The time step interval for the propagation of Eq. (1) in the main text is 10 as. The electron-phonon self energy of Eq. (2) is one of the most expensive parts of the simulation and is calculated in steps of 0.5 fs.

The time–dependent Kerr angle. The matrix elements of the dielectric tensor, ε_{ij}, can be written as

$$\varepsilon_{ij}\left(\omega,\tau\right)=\delta_{ij}-\sum_{l}R_{i,l}^{*}\left(\tau\right)L_{lm}\left(\omega\right)R_{j,m}(\tau), \tag{13}$$

with

$$R_{i,l}\left(\tau\right)=\lim_{\mathbf{q}\to\mathbf{0}}\left(\frac{O_{l}\left(\mathbf{q}\right)}{\left|\mathbf{q}\right|}\right)\sqrt{f_{l}\left(\tau\right)}, \tag{14}$$

and $O_l\left(\mathbf{q}\right)=\langle u_{n\mathbf{k}}|u_{m\mathbf{k}-\mathbf{q}}\rangle$ is the overlap between the periodic parts (u) of the two electronic wavefunctions. In Eq.(13) L_{lm} is the electron–hole response function.[S16] In this work, we use the independent–particle approximation to calculate the Kerr angle.

Generation of a non-equilibrium valley population.

Figure S4 shows the carrier dynamics under the excitation of a circularly polarized pulse and in the absence of any dissipation mechanism. The valley population is defined as the $\mathbf{k}$ integral of the band occupation performed in a spherical area around each $K^{\pm}$ point of radius $0.15\,A^{-1}$. The population is summed over all valence and conduction bands participating in the dynamics. Without dissipation effects, almost all the carriers are photo–excited in the K^{+} valley, with a population in the K^{-} valley three orders of magnitude smaller.[S17] The non–zero population of the K^{-} valley is caused by the fact that the pseudospin is a good quantum number only at K^{+} and K^{-}, while the surrounding regions have a small admixture

of the opposite pseudospin. In the inset we represent the total number of carriers (solid red line), and the pulse intensity (blue shadow). The simulation correctly conserves the total number of electrons during all the dynamics. As expected the total number of photo–excited carriers becomes constant once the pump pulse has turned to zero (around 500 fs).

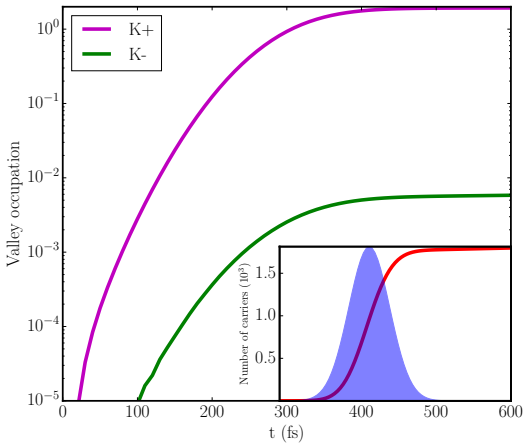

Figure S4: Inset: Photo-generated carriers (red line) and intensity pulse (shadow area) photo–excited by a circular pump pulse (see text) without including any dissipation mechanism. Main panel: Valley occupation in logarithmic scale.

Kerr angle and dielectric function

In the small angle limit the Kerr angle is proportional to the off-diagonal part of the dielectric function, $\varepsilon_{xy}(\omega, \tau)$. It thus depends on the probe frequency and the time delay. In general, the experimental setup imposes the pump and probe frequencies to be energetically close to the optical band gap. In order to determine the temporal evolution of the Kerr angle, we have followed the evolution of the maximum of $\varepsilon_{xy}(\omega, \tau)$ at each time τ. Figure S5 shows $\varepsilon_{xy}(\omega, \tau)$ for several times, at logarithmic scale, for $T = 300\,\mathrm{K}$. The structure of $\varepsilon_{xy}(\omega, \tau)$ consists of a single peak around the pump frequency. Excitations at larger energies could populate a wider energy range and therefore give a more structured spectrum. For the Kerr rotation study in this paper, we have chosen to fix the pump pulse frequency to the maximum of the Kerr angle. This has been done in order to mimic the experiments where the pump

frequency has also been tuned such as to yield maximal Kerr rotation.

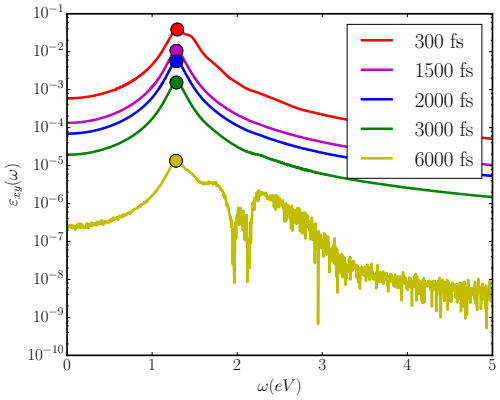

Figure S5: Kerr angle as a function of frequency for probe delay times of τ = 300, 1500, 2000, 3000 and 6000 fs.

The electron-hole exchange mechanism

The electron-hole exchange (eh-X) mechanism[S18] is obtained: (a) by propagating the two-particle density matrix under the effect of the EH-X interaction and (b) assuming an initial state where EH pairs are created only in one valley K.

In our approach, the eh-X interaction is included within the variation of the SEX self-energy. It is indeed responsible (together with electron-hole direct interaction) for shifting the absorption of the pump pulse from the independent-particles to the exciton energies. After the pump pulse has been absorbed, there exists no residual EH-X interaction between the created excitons, i.e., the exciton is an eigenstate of the excitonic Hamiltonian. Thus no eh-X mechanism can exist.

The reason why it exists in the work of Yu and Wu[S18] is assumption (b). Their initial state is not an exciton, i.e., not an eigenstate of the excitonic Hamiltonian, and evolves in time. This is however a fictitious dynamics. If they had properly considered that the pump pulse creates excitons, which can be generated in both valleys, as shown in Fig. S4, no dynamics would exist.

Even accepting assumption (b), the sole dynamics induced by the eh-X mechanism would

be a valley polarization oscillating in time, with electrons jumping back and forth in between K and K'. The authors in Ref.[S18] need to add an external parameter τ_s, which they justify as exciton-exciton scattering mechanism. It is the latter which makes the valley polarization decay. Exciton-exciton scattering however depends on the exciton density and is negligible at low pumping intensities.

Moreover, the long range part of the exchange interaction is pointed out as the dominant term. It is a macroscopic term which has been strongly discussed in the literature for 3D systems. It originates from the non-analytic behaviour of the bare Coulomb interaction at $q = 0$.[S19] However, in systems with reduced dimensionality, such as 2D-materials, this term is zero.[S20,S21]

Last but not least, as we comment in the manuscript, the Hamiltonian entering the eh-X mechanism is temperature independent. The only way temperature could enter is via the thermal distribution of excitons (or their spin). However excitons (or their spin) cannot be thermalized on such short time-scale. The population created by the pump is not thermalized and no electronic temperature exist. The initial lattice temperature instead is dictated by the environment. It is the latter which describes temperature effects. Temperature enters our simulation through the Bose-Einstein distribution for the phonon-mode occupation.

This is why the electron-hole exchange mechanism cannot be used to explain the transfer of excitons from K to K' on the ps time scale and at low laser intensities. The valley depolarization described in our work is instead a quantitative estimate of the importance of the Elliot-Yafet mechanism[S22] induced by spin-orbit plus electron-phonon (and hole-phonon) scattering. It results in an exciton-phonon scattering. Notice that an exciton-phonon scattering is much more justified than exciton-exciton scattering since: (i) it explains the temperature dependence measured experimentally, and (ii) it does not depend on the pumping intensity.

References

(S1) Giannozzi, P.; Baroni, S.; Bonini, N.; Calandra, M.; Car, R.; Cavazzoni, C.; Ceresoli, D.; Chiarotti, G. L.; Cococcioni, M.; Dabo, I.; Corso, A. D.; Gironcoli, S. d.; Fabris, S.; Fratesi, G.; Gebauer, R.; Gerstmann, U.; Gougoussis, C.; Kokalj, A.; Lazzeri, M.; Martin-Samos, L.; Marzari, N.; Mauri, F.; Mazzarello, R.; Paolini, S.; Pasquarello, A.; Paulatto, L.; Sbraccia, C.; Scandolo, S.; Sclauzero, G.; Seitsonen, A. P.; Smogunov, A.; Umari, P.; Wentzcovitch, R. M. *Journal of Physics: Condensed Matter* **2009**, *21*, 395502.

(S2) Onida, G.; Reining, L.; Rubio, A. *Rev. Mod. Phys.* **2002**, *74*, 601–659.

(S3) Marini, A.; Hogan, C.; Grüning, M.; Varsano, D. *Computer Physics Communications* **2009**, *180*, 1392 – 1403.

(S4) Rozzi, C. A.; Varsano, D.; Marini, A.; Gross, E. K. U.; Rubio, A. *Phys. Rev. B* **2006**, *73*, 205119.

(S5) Echeverry, J. P.; Urbaszek, B.; Amand, T.; Marie, X.; Gerber, I. C. *Phys. Rev. B* **2016**, *93*, 121107.

(S6) Qiu, D. Y.; da Jornada, F. H.; Louie, S. G. *Phys. Rev. Lett.* **2013**, *111*, 216805.

(S7) Molina-Sánchez, A.; Hummer, K.; Wirtz, L. *Surface Science Reports* **2015**, *70*, 554 – 586.

(S8) Attaccalite, C.; Grüning, M.; Marini, A. *Phys. Rev. B* **2011**, *84*, 245110.

(S9) Marini, A. *Journal of Physics: Conference Series* **2013**, *427*, 012003.

(S10) de Melo, P. M. M. C.; Marini, A. *Phys. Rev. B* **2016**, *93*, 155102.

(S11) Stefanucci, G.; van Leeuwen, R. *Nonequilibrium Many-Body Theory of Quantum Systems*; Cambridge University Press, 2013.

(S12) Sangalli, D.; Marini, A. *EPL (Europhysics Letters)* **2015**, *110*, 47004.

(S13) Marini, A.; Poncé, S.; Gonze, X. *Phys. Rev. B* **2015**, *91*, 224310.

(S14) Qiu, D. Y.; Cao, T.; Louie, S. G. *Phys. Rev. Lett.* **2015**, *115*, 176801.

(S15) Antonius, G.; Louie, S. G. *arXiv:1705.04245* **2017**,

(S16) Sangalli, D.; Dal Conte, S.; Manzoni, C.; Cerullo, G.; Marini, A. *Phys. Rev. B* **2016**, *93*, 195205.

(S17) Cao, T.; Wang, G.; Han, W.; Ye, H.; Zhu, C.; Shi, J.; Niu, Q.; Tan, P.; Wang, E.; Liu, B.; Feng, J. *Nat Commun* **2012**, *3*, 887–.

(S18) Yu, T.; Wu, M. W. *Phys. Rev. B* **2014**, *89*, 205303.

(S19) Del Sole, R.; Fiorino, E. *Phys. Rev. B* **1984**, *29*, 4631–4645.

(S20) Marinopoulos, A. G.; Reining, L.; Olevano, V.; Rubio, A.; Pichler, T.; Liu, X.; Knupfer, M.; Fink, J. *Phys. Rev. Lett.* **2002**, *89*, 076402.

(S21) Nicholls, R. J.; Perkins, J. M.; Nicolosi, V.; McComb, D. W.; Nellist, P. D.; Yates, J. R. *Journal of Physics: Conference Series* **2012**, *371*, 012060.

(S22) Wu, M.; Jiang, J.; Weng, M. *Physics Reports* **2010**, *493*, 61 – 236.